An *ab initio* study of magnetic relaxation in a dysprosocenium single-molecule magnet

Rizwan Nabi,[a,#] Benjamin E. Atkinson,[b,#] Jakob K. Staab,[a] Jonathan M. Skelton[a,*] and Nicholas F. Chilton[a,b,*]

[a] Department of Chemistry, The University of Manchester, Manchester, M13 9PL, UK

[b] Research School of Chemistry, The Australian National University, Canberra, ACT, 2601, Australia

[#] These authors contributed equally to this work.

Email: jonathan.skelton@manchester.ac.uk, nicholas.chilton@anu.edu.au

Abstract

The development of technologies exploiting molecular spins, such as single-molecule magnets (SMMs) and molecular qubits, requires detailed knowledge of the microscopic spin-dynamics, which in turn relies on understanding the spin-phonon coupling. Building on our recent work, we perform *ab initio* calculations of the phonon modes, anharmonic phonon scattering and spin-phonon coupling in a molecular crystal of the dysprosocenium SMM $[DyCp^{ttt}_2][B(C_6F_5)_4]$. Spin-dynamics simulations give excellent agreement with experiment and provide further insight into the high-performance of the dysprosocenium class of SMMs. We find that strong phonon scattering in the (pseudo-)acoustic regime leads to very short phonon lifetimes, large phonon linewidths, and, consequently, slower spin relaxation.

Introduction

Molecular spins are a powerful platform for exploring the limits to which we can build the smallest possible arbitrarily-configurable magnetic materials, with applications to high-density data storage and quantum computing.[1–3] A fundamental challenge in the area of single-molecule magnetism (SMM) is to raise the maximum temperature at which they exhibit magnetic memory. Currently, the highest temperature at which magnetic hysteresis has been observed is 80 K, in two Dy(III)-based SMMs, *viz.* $[(Cp^{iPr5})Dy(Cp^{*})][B(C_6F_5)_4]$ and $[(Cp^{iPr5})DyI_3Dy(Cp^{iPr5})]$, with fully substituted cyclopentadienyl ligands (Cp^{iPr5} = $C_5(CH(CH_3)_2)_5$, Cp^{*} = $C_5(CH_3)_5$).[4,5] In both systems, the pseudo-linear disposition of the cyclopentadienyl anions creates large axial magnetic anisotropy, and $[(Cp^{iPr5})DyI_3Dy(Cp^{iPr5})]$

also features strong exchange coupling arising from a 5*d* half σ-bond between the two Dy(III) ions, which is thought to be the origin of its ultrahard magnetic coercivity.

Since the magnetic relaxation (i.e. loss of magnetic memory) is driven by spin-phonon coupling through two-phonon Raman scattering and single-phonon Orbach mechanisms, a crucial component of improving performance is understanding the spin-phonon coupling in SMMs.[6–9] The Orbach mechanism is a single-phonon process whose characteristic time has an exponential temperature dependence $\tau = \tau_0 \exp\left(\frac{U_{\text{eff}}}{k_B T}\right)$, where τ_0 is the characteristic time scale of the phonon bath and U_{eff} is the energy barrier.[1] At high temperature, SMMs reverse their magnetisation over the U_{eff} barrier *via* scattering with high-energy optical phonons, but this mechanism is suppressed at low temperatures when the population of these phonons is limited. At lower temperatures, magnetic relaxation is instead dominated by the two-phonon Raman-I process, driven by scattering with low-energy (pseudo-)acoustic phonons.[6–8] Understanding the nature of the phonons in molecular crystals and the interplay of these mechanisms is thus crucial to controlling magnetic relaxation in SMMs.

To this end, we have developed open source software packages to perform *ab initio* calculations of spin-phonon magnetic relaxation dynamics in the solid state,[8–12] and have demonstrated excellent agreement with experiments for Dy(III) SMMs in the crystalline[9] and amorphous solid phases.[13] Here we deploy our methods to study the magnetic relaxation in crystalline $[DyCp^{ttt}_2][B(C_6F_5)_4]$ (**1**),[14] including *ab initio* calculation of the phonon linewidths. We find that strong phonon scattering at low temperature leads to shorter than expected phonon lifetimes, and hence larger phonon linewidths, which partially contributes to the suppression of Raman relaxation at low temperature. This suggests a possible route to slowing two-phonon Raman spin-dynamics in molecular materials by enhancing the low-energy phonon scattering.

Methods

We used density-functional theory (DFT) with VASP 5.4.4[15–18] to obtain an optimised crystal structure and evaluate the solid-state phonon modes, using the PBE functional[19] with the semi-empirical DFT-D3 dispersion correction[20] and projector augmented-wave (PAW) pseudopotentials including a 4f-in-core potential for Dy.[21,22] We used a plane-wave basis set with an energy cutoff of 850 eV and sampled the electronic structure at the Γ-point, justified by convergence of single-point energy and stress calculations. Starting from the primitive cell of **1** obtained from the Cambridge Structural Database (CCDC 2046705),[23] the atomic

positions and unit cell parameters were optimised, maintaining the experimental unit cell volume, to total energy and force tolerances of 10^{-8} eV and 0.01 eV Å^{-1}. Phonons were calculated with Phonopy[24] from force constants evaluated in a 2×2×1 supercell. Third-order force constants were then calculated in the primitive cell using Phono3py.[25] Including all pairwise atomic displacements would require more than 2.7 million single-point calculations, so we employed various distance cutoffs of $3 < r_{cut} < 7$ Å, in steps of 0.5 Å beyond which the pair-wise third-order force were assumed to be zero. This reduces the number of single-point computations to between 63,468 (r_{cut} = 3 Å) and 674,244 (r_{cut} = 7 Å). Linewidths were calculated using second-order perturbation theory on q-point grids with up to 5×5×5 subdivisions.

We used our established protocol for calculating the molecular spin-phonon coupling in the crystalline phase.[8,9,26] In this approach, we perform molecular state-average complete active space self-consistent field spin-orbit (SA-CASSCF-SO) calculations on a single cation of **1** surrounded by a spherical cluster of unit cells (approximate radius 30 Å, chosen by convergence testing). Molecules in the vicinity of the reference molecule are represented by point charges determined from gas-phase DFT calculations on each unique molecule, using Gaussian 09d,[27] with Dy substituted with Y to avoid a multiconfigurational ground state, and fitting the external molecular electrostatic potential using the CHELPG method.[28] The cluster is then embedded in a spherical conductor (Kirkwood solvent model with $\varepsilon \rightarrow \infty$) to screen the unphysical surface charges to accurately reproduce the long-range Madelung potential.[9]

Our SA-CASSCF-SO calculations are performed using OpenMolcas 23.02,[29] considering 18 S = 5/2 states (^{6}H and ^{6}F terms) in a 9-in-7 active space ($4f^9$ configuration) using the second-order Douglas-Kroll-Hess relativistic decoupling,[30] the Cholesky "atomic compact" resolution of the identity method for approximation of two electron integrals,[31] and ANO-RCC basis sets for all atoms (VTZP for Dy, VDZP for the first coordination sphere and VDZ for all other atoms).[32,33] These 18 spin-free states are then mixed with SO coupling, and the electronic states corresponding to the $^6H_{15/2}$ multiplet are projected out of the *ab initio* basis to define the equilibrium Hamiltonian $\hat{H}$ (note that this is not just the lowest 16 Kramers doublets, but the entire angular momentum content of the multiplet). The spin-phonon coupling Hamiltonian for each phonon mode (index j) at each q-point, $\frac{\partial \hat{H}}{\partial Z_{qj}}$, is evaluated using our linear vibronic coupling method,[9,34,35] and the components relevant to the $^6H_{15/2}$ multiplet are projected directly without recourse to a model Hamiltonian.

Magnetic relaxation rates were determined using *TAU*,[8,26] considering both Orbach and Raman-I rate expressions, derived from perturbation theory, given by Equations 1–6 in the supporting information of reference [8]. Calculation of the rates using these perturbative expressions requires an energy gap within the lowest Kramers doublet, which occurs in the experiment due to the presence of a dipolar magnetic field and/or the driving AC magnetic field, and thus we apply a small magnetic field of 2 Oe along the main magnetic axis of the molecule to split the ground doublet by *ca.* 0.02 cm^{-1}. The Raman-I integral is restricted to $\omega < 99$ cm^{-1} to avoid divergence in the perturbation expression, which is sufficiently smaller than the first crystal field excitation of 457.47 cm^{-1} while including sufficient modes populated in the Raman region < 60 K (Figure S1). Integration is performed over antilorentzian phonon lineshapes (Equation 7 in the supporting information of reference [8]) to an equivalent range of $\mu \pm 2\sigma$ (95%) using the trapezoidal method with 100 equidistant steps.

Results and discussion

The crystal structure of **1** has the *P-1* space group and contains a monometallic dysprosocenium cation $[Dy(Cp^{ttt})_2]^+$ and a charge-balancing perfluoronated $[B(C_6F_5)_4]^-$. The structure used here differs from the original in that it does not contain any solvent of crystallisation,[23] but we note that the experimental magnetic relaxation rates are practically identical for the two forms, showing single-phonon Orbach relaxation above 60 K, two-phonon Raman-I relaxation between 50 and 30 K, and quantum tunnelling of the magnetisation (QTM) below 20 K.[23] The asymmetric unit contains one formula unit (Figure 1a), and thus there are two formula units in the primitive unit cell due to the inversion symmetry of the *P-1* space group (Figure 1b), with a total of 276 atoms. The optimised unit cell parameters of **1** are very similar to the experimental ones (Table S1).

The calculated phonon spectrum of **1** contains one small-magnitude imaginary mode at off-Γ *q*-points (Figure 2a). This is likely an artefact of the Fourier interpolation used to obtain frequencies at *q*-points not commensurate with the 2×2×1 supercell expansion, but larger expansions were not computationally viable. The low-energy phonon dispersion and phonon density of states (pDOS) shows a dense band of dispersive modes up to ca. 100 cm^{-1} arising from the pseudo-acoustic modes (external molecular modes, Figure 2).

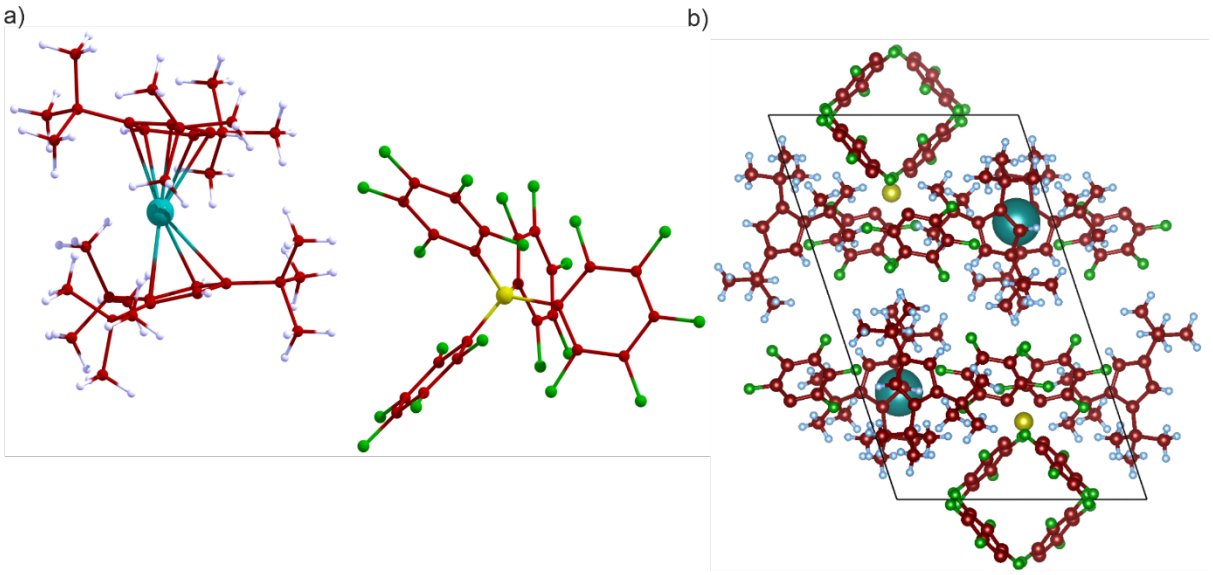

Figure 1. a) Molecular structure of **1**. b) Optimised geometry of the primitive cell containing two molecules. Dy = teal, B = yellow, F = green, C = brown, H = light blue.

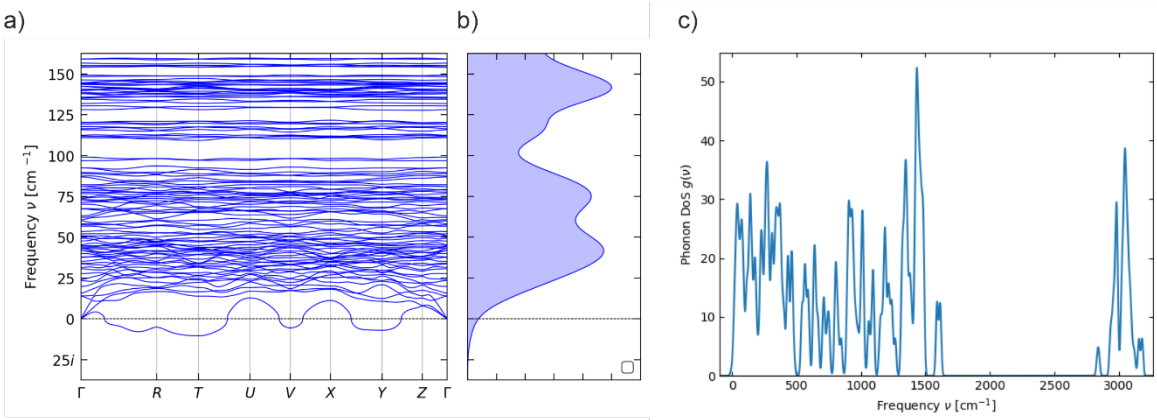

Figure 2. Calculated a) low-energy phonon dispersion and b) density of states (pDOS), and c) full pDOS, of **1**.

We previously found that a 5×5×5 *q*-point mesh in reciprocal space was required to converge the integral over the first Brillouin zone when modelling phonon-driven magnetic relaxation.[9] However, in this case, 4×4×4 and 5×5×5 *q*-point meshes include 30 and 48 imaginary modes, respectively, with frequencies of at most 10.4*i* cm^{-1}, whereas 2×2×2 and 3×3×3 meshes do not have imaginary modes. To test whether the latter are sufficiently converged, we calculated relaxation rates of **1** with up to 5×5×5 using a fixed full-width-at-half-maximum (FWHM) phonon linewidth of 10 cm^{-1}. For the meshes with imaginary frequencies, we tested both neglecting the imaginary modes and setting the frequencies to the absolute values. Magnetic

relaxation rates are practically identical for all tested meshes (Figure S2) and with both treatments of the imaginary frequencies (Figure S3). As such, we can be confident that calculations on 2×2×2 and 3×3×3 meshes are converged with respect to Brillouin zone integration in this case.

Compared to the experimental relaxation rates, the rates calculated using the fixed linewidth of $\Gamma = 10$ cm^{-1} are overestimated across the entire temperature range, but by less than an order of magnitude. Variation of the linewidth from $\Gamma = 0.1$ to 10 cm^{-1} shows a positive correlation with relaxation rate in the Orbach regime and a negative correlation in the Raman-I regime for all of the q-point meshes tested (Figures S4–S10), as observed previously.[9] Comparison to the experimental data hence suggests that the higher-energy optical phonons that drive Orbach relaxation should have a narrower linewidth (ca. Γ = 0.01 cm^{-1}), and the lower-energy (pseudo)acoustic phonons that drive Raman-I relaxation should have a broader linewidth (ca. Γ = 100 cm^{-1}), which is in agreement with DFT calculations of the phonon linewidths (see below).

We also considered the thermodynamic NVT approximation for the linewidths introduced by Lunghi *et al.*[6] In both the Orbach and Raman-I regimes this expression gives rates very similar to those obtained using a fixed $\Gamma = 10$ cm^{-1} (Figures S4-S10), however at higher temperatures the linewidths for the very low energy phonons, which are crucial in the Raman-I regime, become so large that they cause numerical instabilities in the integrals.

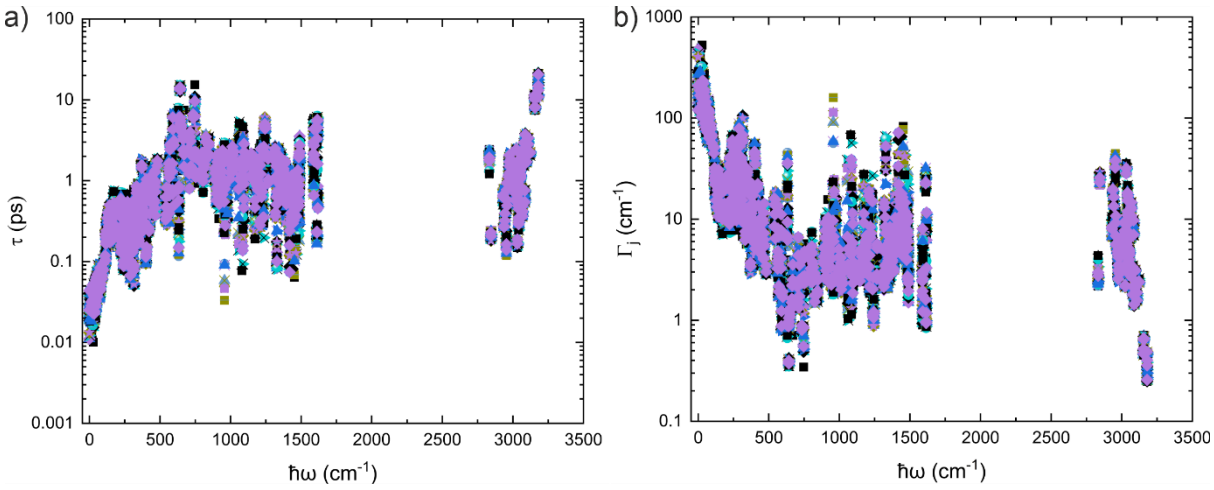

Figure 3. a) Phonon lifetimes and b) linewidths as a function of mode energy at the unique q-points in the 3×3×3 sampling mesh at 300 K. Values for different q-points are shown by different markers and colours.

To calculate the phonon lifetimes and linewidths from first principles requires the three-phonon scattering rates to be determined using the third-order (anharmonic) force constants.[25] Unlike in our previous work on Dy(III) SMM [Dy(bbpen)Br],[9] the present compound **1** has a much lower symmetry crystal structure and more atoms in the unit cell, which makes the calculations far more demanding. We therefore calculated the third-order force constants at different interatomic cutoff distances ($3 < r_{cut} < 7$ Å, see Methods), and determined the phonon lifetimes and linewidths using 2×2×2 and 3×3×3 *q*-point meshes.

The phonon lifetimes at 300 K range from 0.01 to 100 ps, which correspond to linewidths of 500 to 0.05 cm^{-1} (Figures 3 and S11). We observe that the (pseudo-)acoustic modes show a trend of decreasing lifetime with decreasing energy, which is the opposite to what was observed for [Dy(bbpen)Br].[9] As the cutoff is reduced from the largest r_{cut} = 7 Å for the smaller 2×2×2 *q*-mesh, the average difference in the calculated lifetimes at 300 K increases from 0.07 ps (4%) with r_{cut} = 6.5 Å to 0.65 ps (58%) with r_{cut} = 3 Å (Table S2). However, given the orders of magnitude variation in the phonon lifetimes, these averages are not a meaningful metric, and a more useful test is the calculated magnetic relaxation rates. Calculating the rates using the DFT-calculated phonon linewidths at 300 K as a function of r_{cut}, for the 2×2×2 *q*-point mesh, shows that the single-phonon Orbach rates are not greatly influenced by r_{cut} and are similar to the fixed Γ = 10 cm^{-1} calculation (Figure S12b). On the other hand, the two-phonon Raman-I rates show a clear decrease with increasing r_{cut}, closely approaching the experimental rates at r_{cut} = 7 Å (Figure S12a).

However, if we instead use the calculated phonon linewidths at each temperature for which we calculate magnetic relaxation rates, i.e. rather than using the 300 K linewidths at all temperatures, we find that neither the Orbach nor Raman-I rates show a significant dependence on the r_{cut} (Figure S13). Taken together, this implies that the phonon interactions among the low-energy modes are long-ranged at high temperature but become more localised at low temperature; this is likely a consequence of the amplitude (mean-square displacement) of the low-energy modes being strongly dependent on temperature. However, we also find that when accounting for the temperature dependence of the linewidth the rates are very similar to those obtained at a fixed Γ = 10 cm^{-1}, and are overestimated compared to experiment. This suggests that the effective linewidths are *underestimated*, and thus the lifetimes are overestimated, which mirrors our findings in previous work on [Dy(bbpen)Br];[9] we suspect this is partially due to calculations being performed on an infinite perfect crystal compared to a real finite crystal with defects. Using the 300 K linewidths, with an appropriate cutoff, therefore gives

the best results. The same conclusions hold for the rates calculated with r_{cut} = 7 Å and the larger 3×3×3 q-point mesh (Figures 3 and S14).

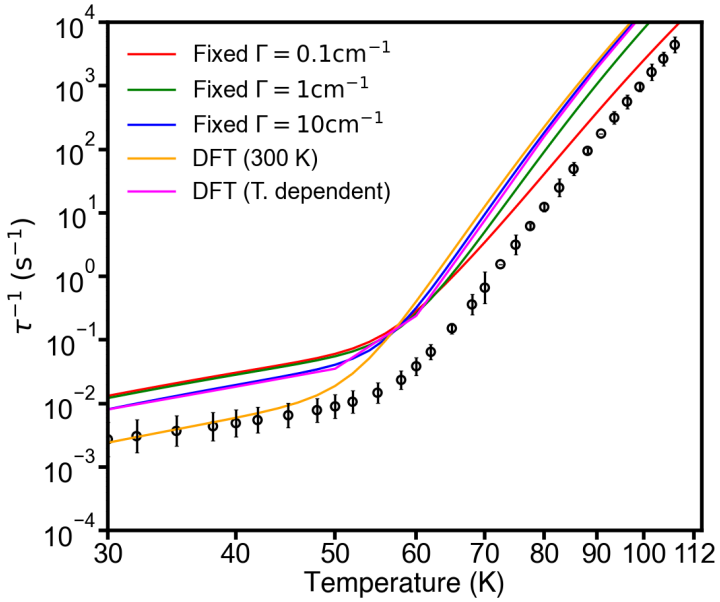

Figure 3. Experimental (black circles) and calculated (solid lines) magnetic relaxation rates of **1**. The calculations are performed on the 3×3×3 q-point mesh with different approximations for the linewidth Γ, *viz.* fixed Γ = 0.1, 1 and 10 cm^{-1} (red, green and blue respectively), and DFT-calculated linewidths at 300 K (orange) and temperature dependent DFT linewidths (pink). DFT-calculated linewidths obtained with r_{cut} = 7 Å.

The calculated spin-phonon coupling and magnetic relaxation shows excellent agreement with the experimental data. The phonon lifetimes for the lowest-energy modes in **1** are as low as 0.01 ps at 300 K, which are an order of magnitude lower than the 0.1 ps in [Dy(bbpen)Br],[9] resulting in far broader linewidths. The variation in phonon linewidths with energy in the low-energy regime also show the opposite trend between the two materials. We note that this finding could not have been obtained with simple fixed linewidth relaxation rate calculations. Remarkably, the rather extreme 10^4 difference in rates at 30 K and ~T^2 vs. ~T^4 temperature dependence of the Raman-I relaxation in **1** and [Dy(bbpen)Br] are accurately captured by our calculations. This suggests that the suppressed Raman-I relaxation in **1** compared to other Dy(III) SMMs can be partially attributed to stronger phonon scattering, leading to shorter phonon lifetimes and broader phonon linewidths, which is related to requirements on the shape of the phonon DoS discussed by some of us previously.[36,37] This in turn indicates that

enhancing phonon scattering by lattice engineering, e.g. by introducing intentional defects or preparing lattice heterostructures, may provide a route to extrinsic enhancement of the spin lifetimes at low temperature.

Acknowledgements

We thank the ERC (STG-851504), The Royal Society (URF191320) and UKRI (MR/T043121/1) for support, and the Computational Shared Facility at The University of Manchester for access to computational resources. This research was undertaken with the assistance of resources and services from the National Computational Infrastructure (NCI), which is supported by the Australian Government. Via our membership of the UK's HEC Materials Chemistry Consortium, which is funded by the UK Engineering and Physical Sciences Research Council (EP/R029431, EP/X035859), this work used the ARCHER2 UK National Supercomputing Service (https://www.archer2.ac.uk).

References

(1) Woodruff, D. N.; Winpenny, R. E. P.; Layfield, R. A. Lanthanide Single-Molecule Magnets. *Chem. Rev.* **2013**, *113* (7), 5110–5148. https://doi.org/10.1021/cr400018q.

(2) Wasielewski, M. R.; Forbes, M. D. E.; Frank, N. L.; Kowalski, K.; Scholes, G. D.; Yuen-Zhou, J.; Baldo, M. A.; Freedman, D. E.; Goldsmith, R. H.; Goodson, T.; Kirk, M. L.; McCusker, J. K.; Ogilvie, J. P.; Shultz, D. A.; Stoll, S.; Whaley, K. B. Exploiting Chemistry and Molecular Systems for Quantum Information Science. *Nat. Rev. Chem.* **2020**, *4* (9), 490–504. https://doi.org/10.1038/s41570-020-0200-5.

(3) Chilton, N. F. Molecular Magnetism. *Annu. Rev. Mater. Res.* **2022**, *52* (1), 79–101. https://doi.org/10.1146/annurev-matsci-081420-042553.

(4) Guo, F.-S.; Day, B. M.; Chen, Y.-C.; Tong, M.-L.; Mansikkamäki, A.; Layfield, R. A. Magnetic Hysteresis up to 80 Kelvin in a Dysprosium Metallocene Single-Molecule Magnet. *Science* **2018**, *362* (6421), 1400–1403. https://doi.org/10.1126/science.aav0652.

(5) Gould, C. A.; McClain, K. R.; Reta, D.; Kragskow, J. G. C.; Marchiori, D. A.; Lachman, E.; Choi, E.-S.; Analytis, J. G.; Britt, R. D.; Chilton, N. F.; Harvey, B. G.; Long, J. R. Ultrahard Magnetism from Mixed-Valence Dilanthanide Complexes with Metal-Metal Bonding. *Science* **2022**, *375* (6577), 198–202. https://doi.org/10.1126/science.abl5470.

(6) Lunghi, A.; Totti, F.; Sessoli, R.; Sanvito, S. The Role of Anharmonic Phonons in Under-Barrier Spin Relaxation of Single Molecule Magnets. *Nat. Commun.* **2017**, *8* (1), 14620. https://doi.org/10.1038/ncomms14620.

(7) Escalera-Moreno, L.; Baldoví, J. J.; Gaita-Ariño, A.; Coronado, E. Spin States, Vibrations and Spin Relaxation in Molecular Nanomagnets and Spin Qubits: A Critical Perspective. *Chem. Sci.* **2018**, *9* (13), 3265–3275. https://doi.org/10.1039/C7SC05464E.

(8) Kragskow, J. G. C.; Mattioni, A.; Staab, J. K.; Reta, D.; Skelton, J. M.; Chilton, N. F. Spin–Phonon Coupling and Magnetic Relaxation in Single-Molecule Magnets. *Chem. Soc. Rev.* **2023**, *52* (14), 4567–4585. https://doi.org/10.1039/D2CS00705C.
(9) Nabi, R.; Staab, J. K.; Mattioni, A.; Kragskow, J. G. C.; Reta, D.; Skelton, J. M.; Chilton, N. F. Accurate and Efficient Spin–Phonon Coupling and Spin Dynamics Calculations for Molecular Solids. *J. Am. Chem. Soc.* **2023**, jacs.3c06015. https://doi.org/10.1021/jacs.3c06015.
(10) Tau. https://gitlab.com/chilton-group/tau.
(11) Angmom_suite. https://pypi.org/project/angmom-suite/.
(12) Spin_phonon_suite. https://pypi.org/project/spin-phonon-suite/.
(13) Staab, J. K.; Rahman, Md. K.; Chilton, N. F. Intramolecular Bridging Strategies to Suppress Two-Phonon Raman Spin Relaxation in Dysprosocenium Single-Molecule Magnets. *Phys. Chem. Chem. Phys.* **2024**, *26* (25), 17539–17548. https://doi.org/10.1039/D4CP01716A.
(14) Goodwin, C. A. P.; Ortu, F.; Reta, D.; Chilton, N. F.; Mills, D. P. Molecular Magnetic Hysteresis at 60 Kelvin in Dysprosocenium. *Nature* **2017**, *548* (7668), 439–442. https://doi.org/10.1038/nature23447.
(15) Kresse, G.; Hafner, J. *Ab Initio* Molecular Dynamics for Liquid Metals. *Phys. Rev. B* **1993**, *47* (1), 558–561. https://doi.org/10.1103/PhysRevB.47.558.
(16) Kresse, G.; Hafner, J. *Ab Initio* Molecular-Dynamics Simulation of the Liquid-Metal–Amorphous-Semiconductor Transition in Germanium. *Phys. Rev. B* **1994**, *49* (20), 14251–14269. https://doi.org/10.1103/PhysRevB.49.14251.
(17) Kresse, G.; Furthmüller, J. Efficiency of Ab-Initio Total Energy Calculations for Metals and Semiconductors Using a Plane-Wave Basis Set. *Comput. Mater. Sci.* **1996**, *6* (1), 15–50. https://doi.org/10.1016/0927-0256(96)00008-0.
(18) Kresse, G.; Furthmüller, J. Efficient Iterative Schemes for *Ab Initio* Total-Energy Calculations Using a Plane-Wave Basis Set. *Phys. Rev. B* **1996**, *54* (16), 11169–11186. https://doi.org/10.1103/PhysRevB.54.11169.
(19) Perdew, J. P.; Burke, K.; Ernzerhof, M. Generalized Gradient Approximation Made Simple. *Phys. Rev. Lett.* **1996**, *77* (18), 3865–3868. https://doi.org/10.1103/PhysRevLett.77.3865.
(20) Grimme, S.; Antony, J.; Ehrlich, S.; Krieg, H. A Consistent and Accurate Ab Initio Parametrization of Density Functional Dispersion Correction (DFT-D) for the 94 Elements H-Pu. *J. Chem. Phys.* **2010**, *132* (15), 154104. https://doi.org/10.1063/1.3382344.
(21) Kresse, G.; Hafner, J. Norm-Conserving and Ultrasoft Pseudopotentials for First-Row and Transition Elements. *J. Phys. Condens. Matter* **1994**, *6* (40), 8245–8257. https://doi.org/10.1088/0953-8984/6/40/015.
(22) Kresse, G.; Joubert, D. From Ultrasoft Pseudopotentials to the Projector Augmented-Wave Method. *Phys. Rev. B* **1999**, *59* (3), 1758–1775. https://doi.org/10.1103/PhysRevB.59.1758.
(23) Parmar, V. S.; Thiel, A. M.; Nabi, R.; Gransbury, G. K.; Norre, M. S.; Evans, P.; Corner, S. C.; Skelton, J. M.; Chilton, N. F.; Mills, D. P.; Overgaard, J. Influence of Pressure on a Dysprosocenium Single-Molecule Magnet. *Chem. Commun.* **2023**, *59* (18), 2656–2659. https://doi.org/10.1039/D2CC06722F.
(24) Togo, A.; Tanaka, I. First Principles Phonon Calculations in Materials Science. *Scr. Mater.* **2015**, *108*, 1–5. https://doi.org/10.1016/j.scriptamat.2015.07.021.
(25) Togo, A.; Chaput, L.; Tanaka, I. Distributions of Phonon Lifetimes in Brillouin Zones. *Phys. Rev. B* **2015**, *91* (9), 094306. https://doi.org/10.1103/PhysRevB.91.094306.

(26) Reta, D.; Kragskow, J. G. C.; Chilton, N. F. Ab Initio Prediction of High-Temperature Magnetic Relaxation Rates in Single-Molecule Magnets. *J. Am. Chem. Soc.* **2021**, *143* (15), 5943–5950. https://doi.org/10.1021/jacs.1c01410.
(27) Frisch, M. J.; Trucks, G. W.; Schlegel, H. B.; Scuseria, G. E.; Robb, M. A.; Cheeseman, J. R.; Scalmani, G.; Barone, V.; Mennucci, B.; Petersson, G. A.; Nakatsuji, H.; Caricato, M.; Li, X.; Hratchian, H. P.; Izmaylov, A. F.; Bloino, J.; Zheng, G.; Sonnenberg, J. L.; Hada, M.; Ehara, M.; Toyota, K.; Fukuda, R.; Hasegawa, J.; Ishida, M.; Nakajima, T.; Honda, Y.; Kitao, O.; Nakai, H.; Vreven, T.; Montgomery, J. A., Jr.; Peralta, J. E.; Ogliaro, F.; Bearpark, M.; Heyd, J. J.; Brothers, E.; Kudin, K. N.; Staroverov, V. N.; Kobayashi, R.; Normand, J.; Raghavachari, K.; Rendell, A.; Burant, J. C.; Iyengar, S. S.; Tomasi, J.; Cossi, M.; Rega, N.; Millam, J. M.; Klene, M.; Knox, J. E.; Cross, J. B.; Bakken, V.; Adamo, C.; Jaramillo, J.; Gomperts, R.; Stratmann, R. E.; Yazyev, O.; Austin, A. J.; Cammi, R.; Pomelli, C.; Ochterski, J. W.; Martin, R. L.; Morokuma, K.; Zakrzewski, V. G.; Voth, G. A.; Salvador, P.; Dannenberg, J. J.; Dapprich, S.; Daniels, A. D.; Farkas, Ö.; Foresman, J. B.; Ortiz, J. V.; Cioslowski, J.; Fox, D. J. Gaussian∼09 Revision D.01.
(28) Breneman, C. M.; Wiberg, K. B. Determining Atom-centered Monopoles from Molecular Electrostatic Potentials. The Need for High Sampling Density in Formamide Conformational Analysis. *J. Comput. Chem.* **1990**, *11* (3), 361–373. https://doi.org/10.1002/jcc.540110311.
(29) Li Manni, G.; Fdez. Galván, I.; Alavi, A.; Aleotti, F.; Aquilante, F.; Autschbach, J.; Avagliano, D.; Baiardi, A.; Bao, J. J.; Battaglia, S.; Birnoschi, L.; Blanco-González, A.; Bokarev, S. I.; Broer, R.; Cacciari, R.; Calio, P. B.; Carlson, R. K.; Carvalho Couto, R.; Cerdán, L.; Chibotaru, L. F.; Chilton, N. F.; Church, J. R.; Conti, I.; Coriani, S.; Cuéllar-Zuquin, J.; Daoud, R. E.; Dattani, N.; Decleva, P.; De Graaf, C.; Delcey, M. G.; De Vico, L.; Dobrautz, W.; Dong, S. S.; Feng, R.; Ferré, N.; Filatov(Gulak), M.; Gagliardi, L.; Garavelli, M.; González, L.; Guan, Y.; Guo, M.; Hennefarth, M. R.; Hermes, M. R.; Hoyer, C. E.; Huix-Rotllant, M.; Jaiswal, V. K.; Kaiser, A.; Kaliakin, D. S.; Khamesian, M.; King, D. S.; Kochetov, V.; Krośnicki, M.; Kumaar, A. A.; Larsson, E. D.; Lehtola, S.; Lepetit, M.-B.; Lischka, H.; López Ríos, P.; Lundberg, M.; Ma, D.; Mai, S.; Marquetand, P.; Merritt, I. C. D.; Montorsi, F.; Mörchen, M.; Nenov, A.; Nguyen, V. H. A.; Nishimoto, Y.; Oakley, M. S.; Olivucci, M.; Oppel, M.; Padula, D.; Pandharkar, R.; Phung, Q. M.; Plasser, F.; Raggi, G.; Rebolini, E.; Reiher, M.; Rivalta, I.; Roca-Sanjuán, D.; Romig, T.; Safari, A. A.; Sánchez-Mansilla, A.; Sand, A. M.; Schapiro, I.; Scott, T. R.; Segarra-Martí, J.; Segatta, F.; Sergentu, D.-C.; Sharma, P.; Shepard, R.; Shu, Y.; Staab, J. K.; Straatsma, T. P.; Sørensen, L. K.; Tenorio, B. N. C.; Truhlar, D. G.; Ungur, L.; Vacher, M.; Veryazov, V.; Voß, T. A.; Weser, O.; Wu, D.; Yang, X.; Yarkony, D.; Zhou, C.; Zobel, J. P.; Lindh, R. The OpenMolcas *Web* : A Community-Driven Approach to Advancing Computational Chemistry. *J. Chem. Theory Comput.* **2023**, *19* (20), 6933–6991. https://doi.org/10.1021/acs.jctc.3c00182.
(30) Reiher, M. Douglas–Kroll–Hess Theory: A Relativistic Electrons-Only Theory for Chemistry. *Theor. Chem. Acc.* **2006**, *116* (1–3), 241–252. https://doi.org/10.1007/s00214-005-0003-2.
(31) Aquilante, F.; Gagliardi, L.; Pedersen, T. B.; Lindh, R. Atomic Cholesky Decompositions: A Route to Unbiased Auxiliary Basis Sets for Density Fitting Approximation with Tunable Accuracy and Efficiency. *J. Chem. Phys.* **2009**, *130* (15), 154107. https://doi.org/10.1063/1.3116784.
(32) Roos, B. O.; Lindh, R.; Malmqvist, P.-Å.; Veryazov, V.; Widmark, P.-O. New Relativistic ANO Basis Sets for Transition Metal Atoms. *J. Phys. Chem. A* **2005**, *109* (29), 6575–6579. https://doi.org/10.1021/jp0581126.

(33) Roos, B. O.; Lindh, R.; Malmqvist, P.-Å.; Veryazov, V.; Widmark, P.-O. Main Group Atoms and Dimers Studied with a New Relativistic ANO Basis Set. *J. Phys. Chem. A* **2004**, *108* (15), 2851–2858. https://doi.org/10.1021/jp031064+.
(34) Staab, J. K.; Chilton, N. F. Analytic Linear Vibronic Coupling Method for First-Principles Spin-Dynamics Calculations in Single-Molecule Magnets. *J. Chem. Theory Comput.* **2022**, *18* (11), 6588–6599. https://doi.org/10.1021/acs.jctc.2c00611.
(35) Staab, J.; Chilton, N. Correction to Analytic Linear Vibronic Coupling Method for First-Principles Spin-Dynamics Calculations in Single-Molecule Magnets. *J. Chem. Theory Comput.* **2024**, *20* (7), 2969–2970. https://doi.org/10.1021/acs.jctc.4c00239.
(36) Chiesa, A.; Cugini, F.; Hussain, R.; Macaluso, E.; Allodi, G.; Garlatti, E.; Giansiracusa, M.; Goodwin, C. A. P.; Ortu, F.; Reta, D.; Skelton, J. M.; Guidi, T.; Santini, P.; Solzi, M.; De Renzi, R.; Mills, D. P.; Chilton, N. F.; Carretta, S. Understanding Magnetic Relaxation in Single-Ion Magnets with High Blocking Temperature. *Phys. Rev. B* **2020**, *101* (17), 174402. https://doi.org/10.1103/PhysRevB.101.174402.
(37) Garlatti, E.; Chiesa, A.; Bonfà, P.; Macaluso, E.; Onuorah, I. J.; Parmar, V. S.; Ding, Y.-S.; Zheng, Y.-Z.; Giansiracusa, M. J.; Reta, D.; Pavarini, E.; Guidi, T.; Mills, D. P.; Chilton, N. F.; Winpenny, R. E. P.; Santini, P.; Carretta, S. A Cost-Effective Semi-Ab Initio Approach to Model Relaxation in Rare-Earth Single-Molecule Magnets. *J. Phys. Chem. Lett.* **2021**, *12* (36), 8826–8832. https://doi.org/10.1021/acs.jpclett.1c02367.